High-gain D-band transmitarrays in standard PCB technology for beyond-5G communications

Francesco Manzillo, Antonio Clemente, José Luis González-Jiménez

This article has been accepted for publication in a future issue of this journal, but has not been fully edited. Content may change prior to final publication. Citation information: DOI 10.1109/TAP.2019.2938630, IEEE Transactions on Antennas and Propagation

High-gain D-band Transmitarrays in Standard PCB Technology for Beyond-5G Communications

Francesco Foglia Manzillo, *Member, IEEE*, Antonio Clemente, *Senior Member, IEEE* and José Luis González-Jiménez, *Senior Member, IEEE*

***Abstract*—We present novel three-layer D-band linearly-polarized transmitarrays entirely fabricated using standard printed circuit board (PCB) processes. Three flat lenses comprising 1600 elements are designed to generate broadside and scanned beams. All lenses are synthesized using 8 unit cells (3-bit phase quantization). The combination of cells comprising probe-fed and aperture-coupled patches is proposed to overcome the design challenges due to technological constraints and achieve a wideband operation. The minimum design feature is 80 μm. The trade-offs in the design of the feed illumination are analyzed using *ad-hoc* numerical tools. A 10-dBi horn is eventually selected as source. The focal-to-diameter (F/D) ratio is 0.75 for all lenses. The broadside array attains a peak gain of 33.0 dBi and a -1-dB relative gain bandwidth of 11.7%, i.e. wider than that of state-of-the-art designs, in the 100-300-GHz band, which use more complex technologies and larger focal distances. The performance of the proposed antenna technology demonstrates its potential for low-cost high-capacity wireless backhauls beyond 100 GHz.**

***Index Terms*—millimeter-wave antennas, transmitarray, discrete lens.**

I. Introduction

THE use of the millimeter-wave (mm-wave) spectrum opens concrete opportunities for future wireless systems to reach unprecedented data-rates. Backhauls operating at D-band (110-170 GHz) may represent the key for enabling massive capacity and ultrahigh-throughput connectivity in small cells of beyond-5G networks. Transmission rates of tens of Gbps in point-to-point links of a few hundred meters [1] could be attained, provided that the antenna gain is >30 dBi and the fractional bandwidths is $>20\%$.

The research for an antenna solution achieving such a performance at frequencies higher than 100 GHz is still at an early stage. Though flat and highly efficient, slotted-waveguide arrays [2] exhibit a limited bandwidth ($\approx 10\%$). Expensive processes, such as diffusion bonding, are employed to achieve the required fabrication accuracy at D-band. Dielectric lens antennas [3]–[5] are the preferred option to ensure high gain over wide frequency ranges. However, being oversized and non-planar, they are unsuited for ultra-dense deployment and tend to exhibit reduced radiation efficiency for very high gain values [5].

Transmitarray antennas [6]–[15] combine the advantages of spatially-fed architectures, e.g. low insertion loss and easy beam-reconfiguration [15], to simple fabrication based on planar processes, such as multilayer PCB technology. Whilst several designs [8]–[10] were successfully demonstrated up to W-band using simple processes and a few metal layers, technological constraints severely limit the antenna performance in the high-end of the mm-wave spectrum (100-300 GHz). The transmitarrays demonstrated in this range [12]–[14] often leverage on more expensive packaging solutions, such as low-temperature co-fired ceramic (LTCC) technology [12]. The unit cells of the LTCC transmitarray in [12] attain a full phase coverage with insertion losses <1 dB from 124 GHz to 158 GHz. However, they comprise 7 metal layers and a large number of vias.

The authors are with CEA - Leti, MINATEC Campus, 38054 Grenoble, France and also with Université Grenoble-Alpes, 38400 Saint-Martin-d'Hères, France (e-mail: {francesco.fogliamanzillo, antonio.clemente, joseluis.gonzalezjimenez}@cea.fr).

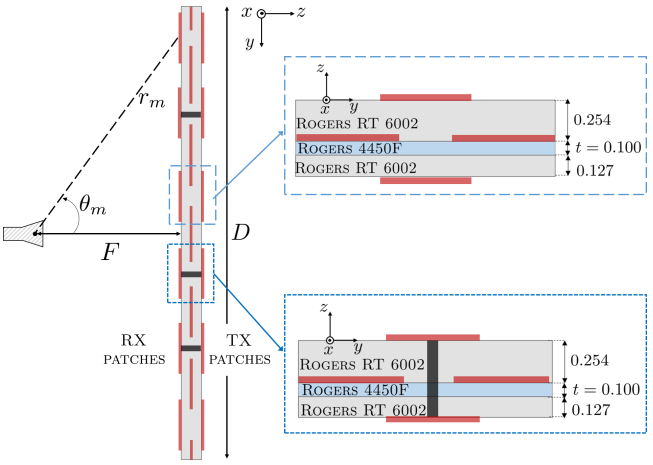

Fig. 1. Transmitarray architecture and stack-ups of the two types of unit cells (aperture-coupled and via-connected patches). Dimensions are in millimeters.

A very few transmitarrays in PCB technology were demonstrated beyond 100 GHz [13], [14]. Due to fabrication constraints, monolithic designs comprise a single substrate and 2 metal layers, which penalizes the -1-dB gain bandwidth (e.g. 6.8% at 250 GHz [13]).

In this paper, we present and experimentally validate a novel design solution to realize broadband, efficient transmitarrays at D-band using standard PCB technology and a reduced number of metal layers. The combination of two types of unit cells in the same radiating aperture is proposed for the first time to overcome the challenges due to the manufacturing constraints and achieve a 360° phase coverage over relative bandwidths exceeding 20%. The two selected cell designs are three-layer *receiving-transmitting* (*Rx-Tx*) antenna structures [6]–[9], where one patch element collect the signal from the feed and a second one re-irradiates it. In the first class of cells, *Rx* and *Tx* elements are aperture-coupled as [7], [9], whereas in the second type, they are directly connected by a via, as in [6], [8].

A 3-bit quantization of the 360° phase range is proposed to attain a small directivity loss (≈ 0.3 dB [8]) and reduce to 8 the number of cells to be simultaneously designed over the targeted band. Nevertheless, as opposed to previously published transmitarrays operating at lower frequencies [8]–[10], the resolution and tolerances of PCB technology make it troublesome to synthesize even a few phase states at D-band, especially using only 3 metal layers. The hybrid design approach here proposed helps to overcome these technological limitations. Eight phase states covering the full phase-range over a 30% -fractional band are achieved exploiting the different behaviors of the two types of cells.

A 40×40 broadside transmitarray based on the designed cells is first presented. The aperture illumination is tailored to attain a gain higher than 30 dBi over a 20%-fractional bandwidth, without resorting to large focal lengths nor to a high-gain primary source. Contrarily to [12], the antenna is relatively compact ($F/D = 0.75$) and the low-gain horn (10-dBi) can be replaced in practical systems

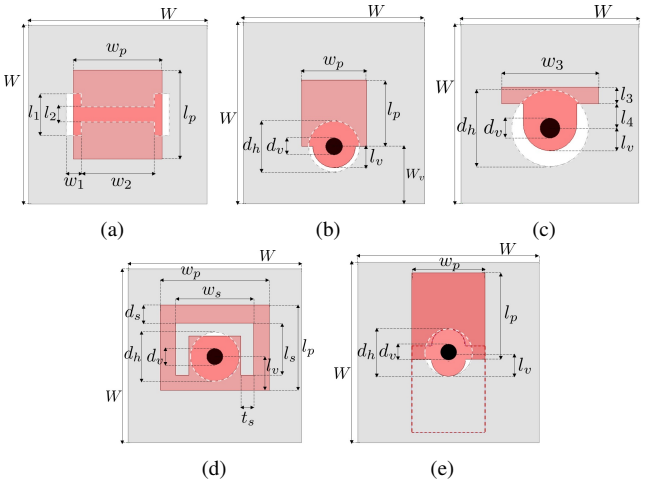

Fig. 2. Unit-cell designs: (a) UC1, UC2, UC3 (aperture-coupled patches); (b) UC4; (c) UC5; (d) UC6; (e) UC7, UC8. The outer patches are shown in red and dashed red lines. The ground plane is depicted in gray, vias in black.

TABLE I
MAIN GEOMETRICAL PARAMETERS OF THE ARRAY CELLS

Design	Cell	Dimensions (mm)
Fig. 2a	UC1	$W = 1.065$, $w_p = 0.53$, $l_p = 0.53$, $l_1 = 0.25$, $l_2 = 0.09$, $w_1 = 0.09$, $w_2 = 0.435$
	UC2	$W = 1.065$, $w_p = 0.465$, $l_p = 0.465$, $l_1 = 0.185$, $l_2 = 0.09$, $w_1 = 0.09$, $w_2 = 0.38$
	UC3	$W = 1.065$, $w_p = 0.410$, $l_p = 0.415$, $l_1 = 0.13$, $l_2 = 0.09$, $w_1 = 0.09$, $w_2 = 0.33$
Fig. 2b	UC4	$W = 1.065$, $w_p = 0.38$, $l_p = 0.39$, $d_h = 0.30$, $d_v = 0.10$, $l_v = 0.13$, $W_v = 0.338$
Fig. 2c	UC5	$W = 1.065$, $w_3 = 0.58$, $l_3 = 0.10$, $l_4 = 0.145$, $l_v = 0.14$, $d_h = 0.46$, $d_v = 0.12$
Fig. 2d	UC6	$W = 1.065$, $w_p = 0.67$, $l_p = 0.52$, $l_s = 0.32$, $l_v = 0.2$, $t_s = 0.08$, $d_s = 0.11$, $d_h = 0.3$, $d_v = 0.1$
Fig. 2e	UC7	$W = 1.065$, $w_p = 0.43$, $l_p = 0.51$, $d_h = 0.28$, $d_v = 0.10$, $l_v = 0.14$
	UC8	$W = 1.065$, $w_p = 0.38$, $l_p = 0.40$, $d_h = 0.28$, $d_v = 0.10$, $l_v = 0.13$

by a small printed array. To the best of our knowledge, this prototype outperforms, in terms of -1-dB gain bandwidth (11.7%), the transmitarrays presented so far in the 100-300-GHz band. Two scanned-beam transmitarays with on-axis feed were also characterized to experimentally assess the scan loss and the performance of the cells under oblique incidence. The results confirm the suitability of the design approach for future developments on beam-steering antennas.

This paper is organized as follows. Section II describes the design and performance of the unit cells. The trade-offs in the design of the transmitarrays are analyzed in Section III. The experimental results are discussed in Section IV. Conclusions are drawn in Section V.

II. DESIGN OF THE UNIT CELLS

Three main objectives were considered in the design of the unit cells: (i) the realization of 8 phase-shifting cells covering the 360° range and operating in a bandwidth wider than 20%; (ii) the use of no more than 3 metal layers to minimize the lens thickness and complexity; (iii) the suitability for standard PCB manufacturing.

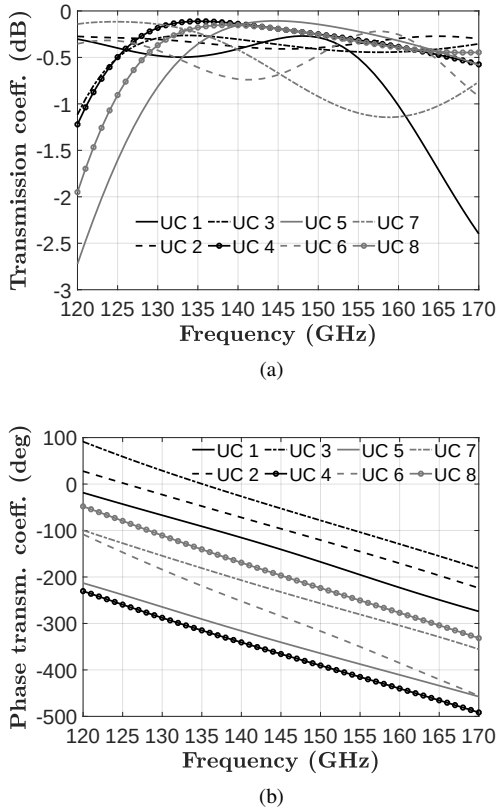

Fig. 3. (a) Amplitude and (b) phase of the transmission coefficients of the cells, simulated under normal incidence in an infinite periodic environment.

These goals are clearly in conflict. For instance, the achievable phase range, as well as the bandwidth, narrows as the thickness and the number of layers of the transmitarray are reduced, leading to degraded aperture efficiency.

Unit cells based on stacked frequency selective structures (FSSs) [10], [11] require at least 4 metal layers to attain a 360° phase coverage and insertion losses < 1 dB, neglecting material losses [16]. In practice, 5 or more layers are commonly employed [10], [11].

Therefore, another class of unit cells, based on coupled *Rx-Tx* antenna elements, is chosen in this work. These structures can be designed to cover the full phase range using only 3 layers [7]–[9]. Furthermore, they are more suitable for electronically-reconfigurable designs [15]. However, the fabrication constraints make the minimum design features electrically large at D-band and severely limit the possibility of devising the frequency responses of the cells. The selected PCB process allows for a minimum width and spacing of conductors of 80 μm. The minimum values of via-diameters and of the distance of via-centers from conductor edges are 100 μm.

A novel design approach is proposed to mitigate these issues. Instead of a single cell design, two different types of *Rx-Tx* cells are employed to achieve 8 broadband phase states over a 360° range. In the first class, *Rx* and *Tx* patches are aperture-coupled, while they are directly connected by a via in the second one. Both cell structures share the same stack-up, shown in Fig. 1, so that the transmitarray can be realized in a single PCB process. It includes 3 metal layers and two Rogers Duroid 6002 substrates ($\epsilon_r = 2.94$, $\tan\delta = 1.2 \times 10^{-3}$) bonded by a Rogers 4450F layer ($\epsilon_r = 3.52$, $\tan\delta = 4.0 \times 10^{-3}$) of nominal thickness $t = 100\,\mu$m. The total thickness, including the copper layers, is 0.515 mm. The *Rx* and *Tx* patches are located on the outer metal layers, while their common ground is on the inner one.

This article has been accepted for publication in a future issue of this journal, but has not been fully edited. Content may change prior to final publication. Citation information: DOI 10.1109/TAP.2019.2938630, IEEE Transactions on Antennas and Propagation

The cell designs are presented in Fig. 2. Cells UC1 to UC3 (see Fig. 2a) comprise aperture-coupled patches. Cells UC4 to UC8 (see Fig. 2b-Fig. 2e) are all based on the second cell structure, with a through-via connecting the patches. The via-connection offers additional parameters to modulate the inter-layer coupling, as compared to the first cell type.

The parallel use of two cell structures enhances the degrees of freedom in the design. It allows the designer to leverage on different coupling mechanisms and tune different sets of parameters for realizing the 3-bit phase quantization while fulfilling the design rules of PCB technology. The fabrication constraints hindered the synthesis of 8 phase states based on the same cell type over a 20%-relative bandwidth. Indeed, a maximum phase range of 180°, i.e. 5 phase states (UC4-UC8), could be attained using cells based on via-connected patches. Design variations to get additional phase states were either unfeasible or too sensitive to tolerances. However, the full phase range was accomplished by designing the 3 remaining cells as aperture-coupled patches (UC1-UC3).

All cells have size $0.5\lambda_0 \times 0.5\lambda_0$, where λ_0 is the free-space wavelength at 140 GHz, and were optimized assuming normal incidence and periodic boundaries. Seven phase states were achieved by tuning the parameters of the 5 designs in Fig. 2. The cell UC8 is obtained from UC4 by mirroring the *Rx* patch with respect to the via, which brings a 180° phase shift [8]. The parameters of the cells are listed in Table I. The simulated transmission coefficients are plotted in Fig. 3. For all cells, the insertion loss (see Fig. 3a) is less than 1 dB between 128 GHz and 153 GHz. The reflection coefficients are less than -8 dB. The average value of the transmission coefficients is > -1 dB in a relative bandwidth of 35.3% at 145 GHz. This provides an estimation of the insertion loss of the transmitarray assuming a uniform illumination and an equiprobable occurrence of each cell. The phases of the transmission coefficients are shown in Fig. 3b. For 6 cells, the relative phase errors with respect to a uniform 3-bit quantization (steps of 45°) are between -10° and 10° from 126 GHz to 158 GHz. The phase error of UC5 is about 20° but very stable against frequency. The relative phase error of UC6 varies from $-25^\circ$to 25°. This degraded response is due to the constraints on the minimum width of the slots on the patches (t_s in Fig. 2d).

By enhancing the design freedom, the proposed approach also helps to improve the robustness to fabrication tolerances. All cells were designed to maintain a good performance when the main geometrical parameters vary around the nominal values according to the tolerances. For instance, the maximum expected misalignment between *Rx* and *Tx* patches with respect to the via-centers is $\pm 40\,\mu$m. Even if this is one of the most critical tolerance, the insertion losses of UC4-UC8 are still < 3 dB between 130 GHz and 160 GHz in the worst case, i.e. for a relative misalignment of the patches of $\pm 80\,\mu$m.

III. Transmitarray Design

The distribution of the cells is determined using an *ad-hoc* tool based on ray tracing and full-wave simulations [6]. The wavefront radiated by the feed is focused in a given direction at the optimization frequency by molding the required phase shift on the array aperture. To this end, the scattering parameters and radiation patterns of the cells are simulated under normal incidence. This is a legitimate assumption for $F/D > 0.6$, i.e. $\theta_m < 40^\circ$ (see Fig. 1), because the responses of the cells are stable in this angular range. Nevertheless, the accuracy is satisfactorily even for shorter focal distances (e.g. $F/D > 0.3$) [6], since only a few cells on the periphery of the array are not correctly modeled and the illumination is tapered. The tool does not accurately estimate the mutual coupling among the transmitarray elements, since each cell is simulated using periodic boundary conditions. A comparison of the results provided by the tool and full-wave simulations is presented in Section IV and proves that the impact of mutual coupling is not relevant.

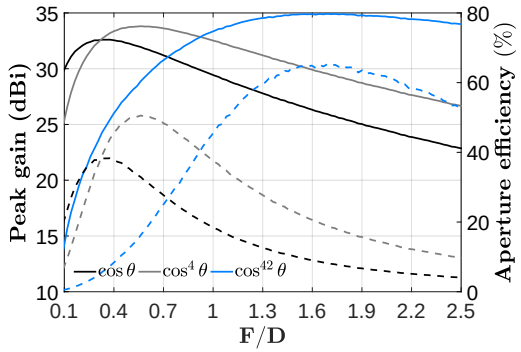

Fig. 4. Peak gain of a 40×40 broadside transmitarray at 137 GHz as a function of focal distance, for different illumination laws.

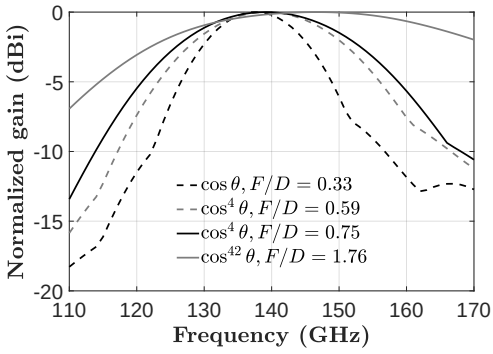

Fig. 5. Normalized gain of a 40×40 broadside transmitarray as a function of frequency, for different sources and focal distances.

The antenna performance strongly depends on the directivity of the feed and its distance from the lens. Low-gain focal sources with broad radiation patterns, as the slot antenna in [10], achieve a quite uniform illumination even at short distances from the lens. However, the angle θ_m subtended by the lens rim at the feed increases for small values of F. Hence, the electrical lengths of the off-axis rays spreading from the feed rapidly vary with the cell position, which results in dispersive designs. On the other hand, directive sources, as the 20-dBi horn in [12], require large focal distances to effectively illuminate the entire aperture. Yet, large F/D values lead to wider bandwidths, since the differences among the distances of the cells from the feed are electrically small in a wider frequency range [17].

These trade-offs were extensively analyzed to design a transmitarray achieving a peak gain of 33 dBi and a -3-dB gain bandwidth of 20% around 140 GHz, using a relatively small F/D ratio. A 40×40 array was considered to reach the desired gain. The maximum gain and the aperture efficiency are plotted against F/D in Fig. 4. The results were obtained using the numerical tool to focus the beam at boresight at 137 GHz. This optimization frequency was selected to center the -3-dB gain bandwidth at 140 GHz. This choice partially compensates the asymmetry of the transmission coefficients of the cells, which degrades faster for frequencies lower than 140 GHz.

Infinitesimal sources with radiation patterns of type $\cos^n \theta$ were assumed as focal feeds. Three relevant values of feed directivity were considered: 6 dBi ($\cos\theta$ pattern), as for the source in [10], 10 dBi ($\cos^4 \theta$) and 20 dBi ($\cos^{42} \theta$) which is close to the gain of the horn exciting the transmitarray in [12]. As expected, the values of F/D maximizing the peak gain increase with the feed directivity. The lens

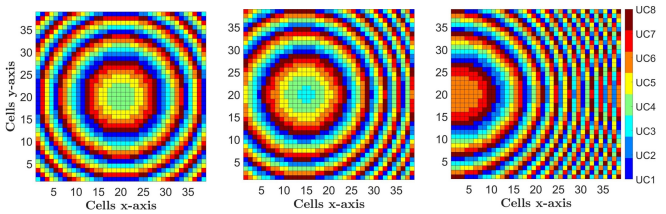

Fig. 6. Cell distributions of the three designed lenses, steering the beam at (a) broadside; (b) 10° in the E-plane and (c) 30° in the E-plane.

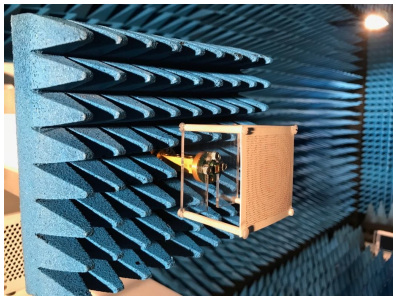

Fig. 7. Antenna under test (broadside lens) in the anechoic chamber.

fed by the $\cos\theta$-source reaches its maximum gain (32.6 dBi) for $F/D = 0.33$, while that optimized for a 20-dBi feed attains 34.9 dBi for $F/D = 1.76$. The 10-dBi source achieves a good compromise between gain and antenna height: 33.8 dBi for F = 24 mm.

The bandwidths of the proposed architectures can be analyzed with the aid of Fig. 5. For each design, the value F maximizing the gain at 137 GHz was considered. The antenna with the most directive feed exhibits the flattest frequency response (-3-dB fractional bandwidths of 34.5%). Instead, when the 10-dBi source and the optimal $F/D = 0.59$ are considered, the -3-dB relative bandwidth is 18.5%. The latter can be further enhanced to fulfill the initial specifications by slightly increasing the focal length. In particular, the -3-dB gain bandwidth of the selected transmitarray design, based on a $\cos^4\theta$-feed, is extended to 21.8% for a valued of $F/D = 0.75$. The choice of a sub-optimal value of F leads to a limited gain drop (from 33.8 dBi to 33.4 dBi).

A linearly-polarized pyramidal horn was employed to get radiation patterns similar to an ideal $\cos^4\theta$ source. The horn has an aperture of size 2.50 mm $\times$ 1.80 mm. Its gain is 9.98 dBi at 140 GHz.

Three 40×40 transmitarrays were designed with the aid of the numerical tool, using the simulated radiation patterns of the horn. All designs were optimized at 137 GHz for $F = 32$ mm. The distributions of the cells in the arrays are shown in Fig. 6. The first one (see Fig.6a) is designed for broadside radiation, while the other two focus the antenna beam in the E-plane at $\theta_0 = 10°$ (see Fig. 6b) and $\theta_0 = 30°$ (see Fig. 6c), respectively.

IV. Experimental Results

A. Broadside transmitarray

Figure 7 shows the broadside transmitarray under test in the mm-wave anechoic chamber. Plastic spacers fix the lens at 32 mm from the horn aperture. Figure 8 compares the measured radiation patterns in the principal planes with those simulated using CST Microwave Studio at the edge and central frequencies of the -3-dB gain band (130 GHz - 160 GHz). An excellent agreement is observed in both planes, except for small discrepancies for frequencies lower than 135 GHz, which can be attributed to fabrication inaccuracies, as discussed later in this section. The beam characteristics are very stable in the band, as shown in Fig. 9 which presents the measured normalized patterns

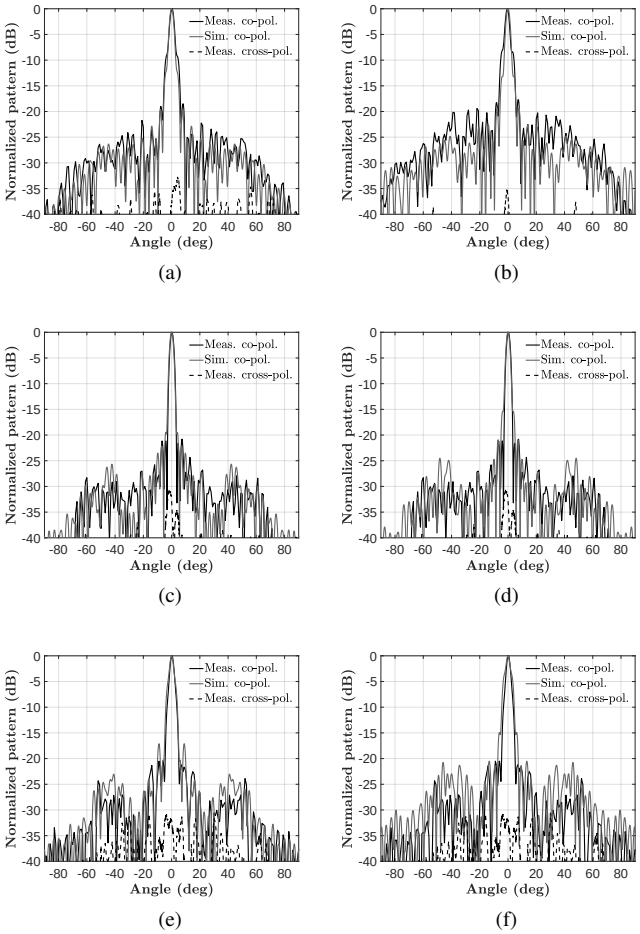

Fig. 8. Simulated and measured radiation patterns of the broadside lens at: (a) 130 GHz, H-plane; (b) 130 GHz, E-plane; (c) 145 GHz, H-plane; (d) 145 GHz, E-plane; (e) 160 GHz, H-plane; (f) 160 GHz, E-plane.

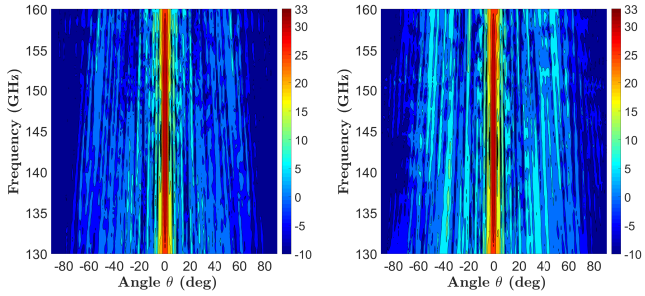

Fig. 9. Measured gain pattern (in dBi) of the broadside lens as a function of frequency and elevation angle. (a) H-plane. (b) E-plane.

in the principal planes as functions of frequency and elevation angle. The measured half-power beamwidth (HPBW) ranges from 2.7° to 3.3° in the E-plane (xz-plane in Fig. 1) and from 2.9° to 3.3° in the H-plane (yz-plane). The average first sidelobe levels (SLLs) between 130 GHz and 160 GHz are -16.3 dB in the E-plane and -18.6 dB in the H-plane. This difference is mainly due to the radiation pattern of the horn, which exhibits different beamwidths in the principal planes. In this frequency range, the peak cross-polarization level is less than -30 dB in both planes. The measured peak gain is plotted

This article has been accepted for publication in a future issue of this journal, but has not been fully edited. Content may change prior to final publication. Citation information: DOI 10.1109/TAP.2019.2938630, IEEE Transactions on Antennas and Propagation

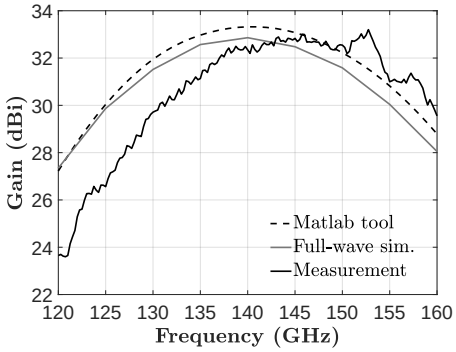

Fig. 10. Measured and simulated gain of the broadside lens versus frequency.

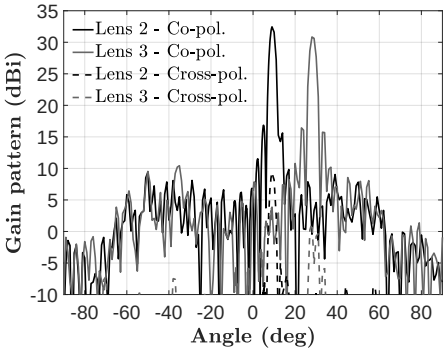

Fig. 11. Measured gain patterns (E-plane cut) at 145 GHz cut of the two beam-steering lens scanning at 10° and 30°, respectively.

against frequency in Fig. 10 and compared to simulated data. The results computed using the *ad-hoc* tool, based on the simulation of the cells in an infinite periodic environment, are in tight agreement with the full-wave simulation of the whole transmitarray, which accounts for actual mutual coupling among the array elements. This shows that, for the present design, mixing the two proposed types of cells in the same finite array does not give rise to significant coupling effects and that the local periodicity approximation provides accurate results. However, the measured gain curve is shifted toward higher frequencies (of about 5 GHz), mainly as a result of fabrication errors (see Section IV-C for more details). Nevertheless, the antenna prototype fulfills the initial bandwidth specification. Indeed, the gain drops of less than 3 dB, with respect to the peak value of 33 dBi, between 130 GHz and 160 GHz, corresponding to a 19.8% relative bandwidth. The measured -1-dB bandwidth ranges from 137 GHz to 154 GHz (11.7%). The aperture efficiency is greater than 25% between 133 GHz to 154 GHz and reaches a maximum of 38.3% at 144 GHz.

B. Scanned-beam transmitarrays

This section presents the performance of the transmitarrays pointing at 10° (Lens 2) and 30° (Lens 3) in the E-plane. As for the broadside lens, the feed is aligned with the center of the lens, at a distance $F = 32$ mm. The E-plane patterns of the two lenses at 145 GHz are shown in Fig. 11. The beam pointing directions are 9.5° (Lens 2) and 28.7° (Lens 3). The gain loss with respect to broadside lens (Lens 1) at the same frequency are 0.45 dB for Lens 2 and 1.9 dB for Lens 3. The E-plane patterns of the two scanned-beam lenses are shown as functions of frequency and elevation angle in Fig. 12. The performance of Lens 2 is stable between 130 GHz and 160 GHz: the scan angle varies from 8.5° to 10.2° and the HPBW from 2.9° to 3.1°. Figure 12b reveals a more pronounced beam squint for Lens 3, which is due to the spatially-fed architecture. The angle of maximum radiation moves closer to boresight as frequency increases: from 32.2° at 130 GHz to 27.0° at 160 GHz. The cross-polarization level is less than -23.5 dB and -27.8 dB for Lens 2 and Lens 3, respectively. The two transmitarrays achieve similar -3-dB gain bandwidths: 133 GHz - 160 GHz. The gain losses with respect to Lens 1 are less than 0.5 dB for Lens 2 and < 2.0 dB for Lens 3.

C. Impact of fabrication errors

The measured gain curves are in line with simulated ones, except for a shift toward higher frequencies. A microscope inspection of the prototypes revealed that the outer patches of the lenses were over-etched. Their dimensions are smaller than the design values of 20 to 30 μm. The impacts of these manufacturing errors on the performance

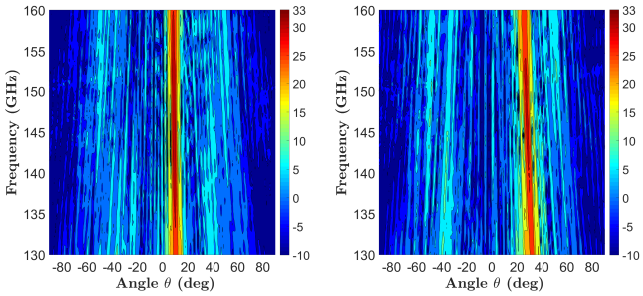

Fig. 12. Measured gain pattern (in dBi) as a function of frequency and elevation angle in the E-plane for the two transmitarrays steering the antenna beam at: (a) $\theta_0 = 10°$ (Lens 2) and (b) $\theta_0 = 30°$ (Lens 3).

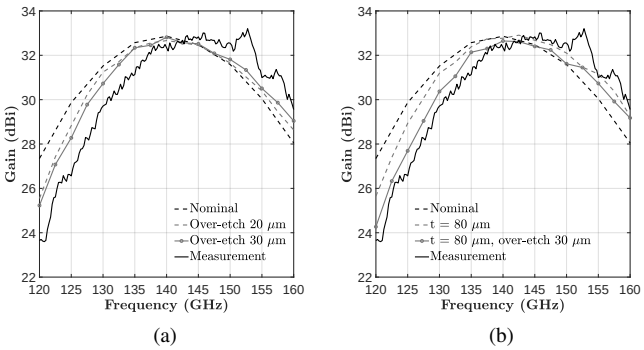

Fig. 13. Tolerance analysis on the broadside lens. Gain versus frequency for (a) a uniform over-etching; (b) different thicknesses t of the pre-preg layer.

were studied by means of simulations. First, a uniform over-etching was assumed. In the simulation model, the dimensions of all metal traces were reduced of a certain quantity, along both axes. At the same time, the dimensions of the slots were increased of the same quantity. The simulated gain is plotted versus frequency in Fig. 13a for two over-etching values (20 μm and 30 μm) and compared to measurements and to the numerical results obtained for the nominal design. The operating band shifts at higher frequencies as the over-etching is more relevant and matches better the measured one.

The thickness of the bonding layer (t in Fig. 1) has also an important impact on the frequency response. It mainly affects the coupling among the patches in cells UC1-UC3. As the materials used in this work are relatively soft, the pre-preg layer is likely to be

TABLE II
COMPARISON WITH STATE-OF-THE-ART MM-WAVE TRANSMITARRAYS

Ref.	[8]	[9]	[10]	[12]	[13]	This work
Freq. (GHz)	61.5	61.5	83.5	140	250	145
Technology	PCB	PCB	PCB	LTCC	PCB	PCB
N. metal layers	3	3	6	7	2	3
Vias	Yes	No	No	Yes	No	Yes
Source gain (dBi)	15	10	≈ 6	20	≈ 6	10
Diameter	$20\,\lambda$	$20\,\lambda$	$25\,\lambda$	$20\,\lambda$	$14\,\lambda$	$20\,\lambda$
F/D	0.70	0.55	0.32	1.87	0.30	0.75
Peak gain (dBi)	32.5	33.4	33.9	33.5	28.8	33.0
-1-dB gain bandwidth	15.4%	10.1%	6.0%	10.7%	6.8%	11.7%
Max. aperture efficiency	42.7%	48.0%	30.8%	50.1%	32.0%	38.3%

thinner than the nominal value ($t = 100\,\mu$m). Figure 13b shows the effects of a smaller t on the gain response of the broadside transmitarray. For $t = 80\,\mu$m, the bandwidth is shifted toward higher frequencies and the gain decay at low frequencies is faster as compared to the nominal design. When an over-etching of $30\,\mu$m and $t = 80\ \mu$m are simultaneously considered, the simulation results (dotted gray curve in Fig. 13b) closely match experimental ones.

D. Comparison with the state of the art

Table II compares the performance of the broadside prototype to state-of-the-art mm-wave transmitarrays. The designs at 60 GHz [8], [9] profit from less stringent fabrication constraints, especially in terms of minimum widths of the slots and via-diameters. Nevertheless, a similar performance is attained at D-band in the present work. The V-band transmitarray in [8], based on via-connected patches, achieves slightly wider bandwidth and higher efficiency, partly due to the optimized illumination provided by the feed.

The E-band via-less FSS-based transmitarray in [10] comprises twice the number of metal layers used in our work. Nonetheless, its -1-dB relative bandwidth is only 6%, since the design focuses on the reduction of the antenna thickness ($F/D = 0.32$).

The D-band transmitarray in [12] leverages LTCC technology to enhance the fabrication resolution. It comprises 7 metal layers. Wideband cells are designed using magneto-electric dipoles as *Rx-Tx* elements and a large number of vias for realizing the phase-shifter. The choice of a highly-directive feed (a 20 dBi horn) and of a very large focal distance ($F/D = 1.87$) further broadens the bandwidth. Nevertheless, the proposed 3-layer transmitarray attains a wider -1-dB bandwidth (11.7% against 10.7%) and a similar gain using a much shorter focal length and a 10-dBi gain horn. Note that the 10-dBi-source used in this work can be replaced by a small and efficient printed antenna, which reduces the overall thickness of the antenna module. Conversely, a high-gain feed, as that in [12], cannot be design as a planar antenna but using large and lossy arrays.

The few transmitarrays in PCB technology reported in the 100-300-GHz band rely on Fabry-Perot cells [13], [14]. The bandwidth of the 2-layer array in [13] (6.8% at 250 GHz) is penalized by the small F/D and the necessity of using a single substrate to avoid further performance degradation due to tolerances in multilayer stack-ups.

V. CONCLUSION

The design and characterization of broadband 3-layer 3-bit transmitarrays in standard PCB technology were presented. The design benefits from the combination in the array of two types of cells, based on either via-connected or aperture-coupled patches, overcoming the challenges due to the manufacturing constraints. This design approach made it possible to achieve a 360°-phase coverage with small phase errors and average insertion loss < 1 dB over a relative bandwidth greater than 30%. Three 40×40 arrays, pointing at boresight, at 10° and 30° in the E-plane, were realized. The trade-offs related to the choice of the feed (a 10-dBi horn) and of the focal length were discussed. The designs were optimized to achieve a relatively small height, paving the way for the realization of low-profile monolithic modules in future works. The size of the transmitarrays is $42.6 \times 42.6 \times 32$ mm^3. The broadside lens exhibits a -1-dB fractional gain bandwidth is 11.7% and a maximum aperture efficiency of 38.3%. The proposed antenna technology represents a cost-effective and efficient solution for beyond-5G wireless front-ends at D-band.

REFERENCES

[1] I. Ando, M. Tanio, M. Ito, T. Kuwabara, T. Marumoto, and K. Kunihiro, "Wireless D-band communication up to 60 Gbit/s with 64-QAM using GaAs HEMT technology," in *IEEE Radio Wirel.Symp.*, Jan. 2016, pp. 193–195.

[2] D. Kim, J. Hirokawa, M. Ando, J. Takeuchi, and A. Hirata, "64×64-element and 32×32-element slot array antennas using double-layer hollow-waveguide corporate-feed in the 120 GHz band," *IEEE Trans. Antennas Propag.*, vol. 62, no. 3, pp. 1507–1512, Mar. 2014.

[3] A. J. Alazemi, H. Yang, and G. M. Rebeiz, "Double bow-tie slot antennas for wideband millimeter-wave and terahertz applications," *IEEE Trans. THz Sci. Technol.*, vol. 6, no. 5, pp. 682–689, Sept 2016.

[4] B. Gottel, M. Pauli, H. Gulan, M. Girma, J. Hasch, and T. Zwick, "Miniaturized 122 GHz short range radar sensor with antenna-in-package (AiP) and dielectric lens," in *Proc. 8th Eur. Conf. Antennas Propag.*, The Hague, The Netherlands, April 2014, pp. 709–713.

[5] J. P. Teixeira *et al.*, "Transmit array as a viable 3D printing option for backhaul applications at V-band," in *Proc. IEEE Int. Symp. Antennas Propag.*, July 2017, pp. 2641–2642.

[6] H. Kaouach, L. Dussopt, J. Lanteri, T. Koleck, and R. Sauleau, "Wideband low-loss linear and circular polarization transmit-arrays in V-band," *IEEE Trans. Antennas Propag.*, vol. 59, no. 7, pp. 2513–2523, July 2011.

[7] A. Abbaspour-Tamijani, K. Sarabandi, and G. M. Rebeiz, "Antenna-filter-antenna arrays as a class of bandpass frequency-selective surfaces," *IEEE Trans. Microw. Theory Techn.*, vol. 52, no. 8, pp. 1781–1789, Aug. 2004.

[8] C. Jouanlanne *et al.*, "Wideband linearly polarized transmitarray antenna for 60 GHz backhauling," *IEEE Trans. Antennas Propag.*, vol. 65, no. 3, pp. 1440–1445, Mar. 2017.

[9] L. Dussopt *et al.*, "A V-band switched-beam linearly polarized transmit-array antenna for wireless backhaul applications," *IEEE Trans. Antennas Propag.*, vol. 65, no. 12, pp. 6788–6793, Dec. 2017.

[10] Y. Kasahara, M. Wu, K. Kosaka, H. Toyao, E. Hankui, and A. Alú, "Low-profile transmitarray antenna with single slot source and metasurface in 80-GHz band," in *Proc. IEEE Int. Antennas Propag. Symp.*, July 2018, pp. 521–522.

[11] M. Li, M. A. Al-Joumayly, and N. Behdad, "Broadband true-time-delay microwave lenses based on miniaturized element frequency selective surfaces," *IEEE Trans. Antennas Propag.*, vol. 61, no. 3, pp. 1166–1179, Mar. 2013.

[12] Z. W. Miao et *al.*, "140 GHz high-gain LTCC-integrated transmit-array antenna using a wideband SIW aperture-coupling phase delay structure," *IEEE Trans. Antennas Propag.*, vol. 66, no. 1, pp. 182–190, Jan. 2018.

[13] H. Yi, S. W. Qu, and C. H. Chan, "Low-cost two-layer terahertz transmit array," *Electron. Lett.*, vol. 53, no. 12, pp. 789–791, 2017.

[14] S. Qu, H. Yi, B. J. Chen, K. B. Ng, and C. H. Chan, "Terahertz reflecting and transmitting metasurfaces," *Proc. IEEE*, vol. 105, no. 6, pp. 1166–1184, Jun. 2017.

[15] A. Clemente, L. Di Palma, F. Diaby, L. Dussopt, T. K. Pham, and R. Sauleau, "Electronically-steerable transmitarray antennas for Ka-band," in 13th *Eur. Conf. Antennas Propag.*, Krakow, Poland, Apr. 2019.

[16] A. H. Abdelrahman, A. Z. Elsherbeni, and F. Yang, "Transmission phase limit of multilayer frequency-selective surfaces for transmitarray designs," *IEEE Trans. Antennas Propag.*, vol. 62, no. 2, pp. 690–697, Feb. 2014.

[17] Y. Rahmat-Samii, "Reflector antennas," in *Antenna Handbook*, Y. Lo and S. W. Lee, Eds. New York: Van Nostrand Reinhold, 1988.